TWENTY-FIFTH EUROPEAN ROTORCRAFT FORUM

Paper n° G14

VIBRATION SUPPRESSION IN HELICOPTERS WITH THE ACSR APPROACH USING AN IMPROVED CONTROL ALGORITHM

BY

R. CRIBBS, P. P. FRIEDMANN
UNIVERSITY OF MICHIGAN, USA

SEPTEMBER 14 - 16, 1999
ROME
ITALY

ASSOCIAZIONE INDUSTRIE PER L'AEROSPAZIO, I SISTEMI E LA DIFESA
ASSOCIAZIONE ITALIANA DI AERONAUTICA ED ASTRONAUTICA

VIBRATION SUPPRESSION IN HELICOPTERS WITH THE ACSR* APPROACH USING AN IMPROVED CONTROL ALGORITHM

R. Cribbs† and P.P. Friedmann‡
Department of Aerospace Engineering
University of Michigan
Ann Arbor, Michigan 48109-2140

ABSTRACT

This paper describes vibration modeling and control using a coupled rotor/fuselage aeroelastic response model with refined aerodynamics. The flexible fuselage, modeled by a three-dimensional structural dynamic finite element model, is combined with a flexible, four-bladed hingeless rotor. The unsteady aerodynamic loads are obtained from a free wake model combined with rotor/fuselage aerodynamic interaction effects. The effects of the various aerodynamic refinements on vibratory loads and fuselage accelerations are studied. Vibration reduction with active control of structural response (ACSR) is carried out with two control algorithms. The improved control scheme is capable of tailoring the vibration reduction process so as to produce low accelerations at locations of particular interest such as the pilot seat. Results indicate a large increase in vibratory loads and fuselage accelerations when using the refined aerodynamic model. Though both control methods reduce airframe vibrations, the improved control algorithm provides significantly lower accelerations when compared to the basic control algorithm with similar actuator requirements.

NOMENCLATURE

a	Blade lift curve slope
a_x, a_y, a_z	Fuselage longitudinal, lateral, and vertical accelerations at various locations
c_b	Blade chord
c_p	Coefficient of pressure
$\mathbf{C}_O, \mathbf{C}_I, \mathbf{C}_{NW}$	Matrices of induced velocity influence coefficients
C_T	Rotor coefficient of thrust
C_W	Helicopter coefficient of weight
$\mathbf{D}$	Wake distortion
EI_y, EI_z	Blade bending stiffnesses in flap and lead-lag
$\mathbf{F}_b^A, \mathbf{F}_b^G, \mathbf{F}_b^I$	Blade aerodynamic, gravitational, and inertial forces
$\mathbf{F}_{b_o}, \mathbf{F}_{b_{nc}}, \mathbf{F}_{b_{ns}}$	Fourier coefficients of blade equations of motion
fC_{df}	Fuselage equivalent flat plate drag area
$\mathbf{F}_{fus}$	Total fuselage forces
F_x, F_y, F_z	Vibratory hub shear components
GJ	Blade torsional stiffness
h	Rotor hub length
I_x, I_y, I_z	Fuselage moments of inertia about the center of mass
J	Quadratic control performance index
m_b	Blade mass distribution per unit length
$\mathbf{M}_b^A, \mathbf{M}_b^G, \mathbf{M}_b^I$	Blade aerodynamic, gravitational, and inertial moment

*Active Control of Structural Response
†Postdoctoral Scholar
‡François-Xavier Bagnoud Professor of Aerospace Engineering

$\mathbf{M}_{fus}$	Total fuselage moments
M_x, M_y, M_z	Vibratory hub moment components
N_b	Number of blades
p	pressure
$\mathbf{q}$	Response vector
$\mathbf{r}_w$	Position of wake element
R	Rotor radius
$\mathbf{T}$	Jacobian of the acceleration response with respect to the current control input
$\vec{u}$	Vector of control amplitudes
$\vec{u}^*$	Optimal control vector
$\|V\|$	Magnitude of air velocity
$\mathbf{W_u}, \mathbf{W_z}$	Weighting matrices on the control amplitudes and acceleration amplitudes, respectively
x	Blade spanwise coordinate
X_{FA}, Z_{FA}	X and z locations of the fuselage aerodynamic center relative to fuselage/hub intersection
X_{FC}, Z_{FC}	X and z locations of the fuselage center of mass relative to fuselage/hub intersection
$\vec{z}$	Vector of selected airframe acceleration amplitudes
α_R	Rotor trim pitch angle
β_p	Blade precone angle
γ	Lock number
Γ_I, Γ_O	Inboard and outboard circulation peaks defining the strength of the tip vortices
Γ_{ij}	Bound vorticity at azimuth j and spanwise location i
$\theta_o, \theta_{1c}, \theta_{1s}$	Blade collective pitch, cyclic cosine and sine pitch angles, respectively
θ_{tr}	Tail rotor collective pitch angle
λ	Non-dimensional induced velocity
μ	Advance ratio
ρ_A	Air density
σ	Rotor solidity ratio
ϕ_V	Velocity potential
ϕ_s	Rotor trim roll angle
ψ	Blade azimuth angle or non-dimensional time ($= \Omega$ t)
Ω	Angular speed of rotor

1 INTRODUCTION

One of the primary concerns in rotorcraft design is the issue of vibrations and its reduction. In recent years, requirements for vibrations in military helicopters have been established that limit vibration levels to 0.05g at certain fuselage locations. High levels of vibration lead to passenger discomfort, increased noise levels and fatigue of both pilot and aircraft which in turn decrease rotorcraft performance and increase cost. These issues are critical to the acceptance of rotorcraft, thus, the issues of vibration prediction and its reduction to acceptable levels are of primary importance to the rotorcraft designer.

The largest contributor to vibrations in a helicopter is the rotor. The rotor blades transfer vibratory loads from the hub to the fuselage at harmonics that are predominantly N_b/rev, where N_b is the number of blades. Blade vortex interactions (BVI) and rotor/fuselage interference effects add complexity to the vibratory loading environment. In order to determine the vibration levels at various fuselage locations, it is necessary to consider a coupled rotor/flexible fuselage model. Studies by Yeo and Chopra [1] have shown remarkable differences in vibration levels in a coupled rotor/flexible fuselage system when using linear inflow and comparing it to free wake models. At certain advance ratios, the loads obtained when using the free wake model resulted in vibration levels that were 100 times higher than those obtained using a linear inflow model. The fuselage model used in Ref. 1 consisted of a "stick" model of the AH-1G. Recent analyses [2–4] and wind tunnel investigations [5–7] have shown the influence of rotor/fuselage interaction on rotor loads. But these studies

were mainly concerned with the time averaged phenomena and not the rotor/fuselage interference effects on vibrations. It is thus clear that more accurate aerodynamic models are required in order to predict vibrations, and conduct aeroelastic response simulations for vibration control. Furthermore, the improved aerodynamics should be combined with equally refined structural dynamic models.

Recently, active control strategies have been developed that can reduce vibration levels well below those achieved through traditional passive methods such as dampers and mass tuning [8]. Among the active control approaches, two fundamentally different strategies have emerged. Three approaches: higher harmonic control (HHC), individual blade control (IBC) and the actively controlled flap (ACF) all attempt to control the vibrations, at their source on the rotor blades, by manipulating the unsteady aerodynamic loading in the rotating system. A second promising alternative approach is the active control of structural response (ACSR) where vibrations are reduced by actuators located in the fuselage. In this case, vibration reduction is carried out in the non-rotating system.

A schematic of the ACSR system is shown in Figure 1. Inputs to the actuators excite the fuselage so as to counteract the excitation due to the rotor system. Thus the combined input of the rotor disturbance and the actuator forces is minimized. Since the implementation of this method of vibration control occurs in the non-rotating system, the complexity and airworthiness issues associated with the alternative approaches are eliminated. Also, older aircraft may be retrofitted with the actuators to improve their vibration levels. This approach was initially developed by Staple at Westland [9,10] and was successfully flight tested by both Westland and Sikorsky [11,12]. This approach is currently implemented on a production helicopter, the Westland/Augusta EH101. A mathematical model capable of simulating this vibration reduction approach has been developed by Chiu and Friedmann [13,14] at UCLA. This mathematical model employs simplified aerodynamics for both the rotor and the fuselage. The model used was based on uniform inflow, quasisteady aerodynamics for the blades and a simple flat plate equivalent area model was used for the fuselage aerodynamics. This model neglects rotor/fuselage aerodynamic interference effects.

The present study is aimed at developing an improved understanding into the mechanisms of helicopter vibrations and their control using ACSR. The specific objectives of the paper are: (1) investigate the influence of a new aerodynamic model, that combines a free wake model of the rotor with a model capable of representing rotor/fuselage interactional aerodynamics, on the vibratory loading and resulting fuselage accelerations; (2) development of an improved control algorithm that permits vibration reduction to be preferentially applied to specific fuselage locations; (3) investigate the vibration reduction capabilities of the improved control algorithm; and (4) compare the improved control method accelerations to the results of the basic control algorithm previously studied at UCLA.

2 MATHEMATICAL MODEL

The coupled rotor/flexible fuselage model is capable of representing a helicopter rotor consisting of a number of flexible, hingeless blades combined with a three-dimensional flexible fuselage. The description of the model, given below, is separated into its components; namely, rotor, wake model, fuselage structural model, and fuselage aerodynamic model.

2.1 ROTOR MODEL

The hingeless rotor blade is modeled as a slender, inextensible beam cantilevered at the root. This isotropic blade model, taken from Ref. 15, includes coupled flap-lag-torsional dynamics in the presence of moderate deflections. The distributed aerodynamic, gravitational, and inertial loads per unit length, including the effects of fuselage motion, are combined to obtain the total distributed force and moment acting on the blade. The inertial and aerodynamic loads are derived implicitly.

The aerodynamic loads on the rotor are calculated using quasisteady, Greenberg type aerodynamics combined with a free wake model. The reverse flow region on the blade is accounted for by switching the direction of the drag acting on the cross-section of the blade and setting the lift and moment terms equal to zero inside the reverse flow region. Stall and compressibility effects are neglected.

2.2 WAKE MODEL

The rotor wake model has been extracted from the comprehensive rotorcraft analysis tool, CAMRAD/JA [16, 17], and modified to be compatible with the aeroelastic response analysis employed in our

simulation. It is comprised of a wake geometry model which determines the location of the wake in space and a wake calculation model which, given the wake geometry, calculates the induced velocity distribution.

The free wake geometry scheme was initially developed by Scully [18]. Each wake element is created at the blade and is convected with the air's local velocity which is composed of the free stream velocity and the wake induced velocity. The wake geometry is calculated as follows: first, the positions of the blade generating the wake elements are calculated; second, the undistorted wake is found by adding the contribution of the free stream velocity to the wake element creation points; third, the free wake geometry is found by adding the distortion due to the wake and fuselage induced velocities to the undistorted geometry. A wake element is thus described by the position of blade when the wake element was created and the time elapsed from the time of element creation to the current time, or:

$$\mathbf{r}_w(\psi,\phi) = \mathbf{r}_b(\psi-\phi) + \phi\mathbf{v}_w + \mathbf{D}(\psi,\phi) \tag{1}$$

The wake distortion, $\mathbf{D}(\psi,\phi)$, is calculated by integrating in time the wake and fuselage induced velocities acting on the wake element.

The wake calculation routine was developed by Johnson [19]. The model is based on a vortex lattice approximation of the wake consisting of two main elements: the tip vortex and an inboard vortex sheet. The tip vortex is a concentrated vorticity filament generated at the tip of the blade while the inboard vortex sheet is due to trailed and shed vorticity and is much weaker and more diffuse than the tip vortex. The tip vortices are modeled as vortex lines with small viscous core radii while the inboard sheet can be represented by either vortex sheet elements or vortex line segments with large core radii. Given the wake geometry and the bound circulation distribution, matrices of influence coefficients are calculated. These influence coefficients describe the wake induced velocities as a function of blade bound circulations. A simple matrix multiplication of influence coefficients times the circulation distribution provide the induced velocities as shown:

$$\lambda_i = \sum_{j=1}^{J}\Gamma_{Oj}\mathbf{C}_{Oj} + \sum_{j=1}^{J}\Gamma_{Ij}\mathbf{C}_{Ij} + \sum_{j=0}^{K_{NW}}\sum_{i=1}^{M}\Gamma_{ij}\mathbf{C}_{NW_{ij}} \tag{2}$$

where J and M are the numbers of azimuth and spanwise stations, respectively, at which the induced velocities are calculated and K_{NW} is the number of azimuth stations that describe the extent of the near wake.

2.3 FUSELAGE STRUCTURAL MODEL

The fuselage equations of motion are determined using a Lagrangian formulation. The elastic fuselage is modeled as a three dimensional assemblage of finite elements which allows the elastic displacements to be defined by a finite number of generalized coordinates. The fuselage equations of motion are decoupled into rigid body equations of motion and elastic fuselage equations of motion using a truncated set of fuselage natural modes and mean axes.

The finite element model used to obtain the natural modes and frequencies consists of Euler-Bernoulli beams and non-structural masses to model items such as fuel tanks, payload, transmission, engine, etc... The solution to the complete eigenvalue problem for the model with 966 degrees of freedom is carried out using the IMSL subroutine DGEGV [20].

2.4 FUSELAGE AERODYNAMIC MODEL

An equivalent flat plate area is used to calculate the drag of the fuselage due to viscous and profile effects. To model the influence of the fuselage on the rotor aerodynamic loads, the fuselage is represented by a set of sources/sinks that describe a body of revolution. As described in Ref. 21, a body of revolution resembling a helicopter fuselage in axial flow can be represented by as few as three three-dimensional sources/sinks. The shape of the body of revolution used in this study is shown superimposed on the fuselage structural model in Figure 3. This body of revolution is described by one three-dimensional source and two three-dimensional sinks. Using such a limited number of sources/sinks combination creates a computationally efficient model that is well suited to the complex coupled rotor/fuselage problem.

To satisfy the requirement that air should not penetrate the surface of the fuselage, two-dimensional line sources are distributed about the surface of the body of revolution to enforce that normal velocities at the fuselage surface be zero. These off axis velocities are due to rotor/wake induced velocities and pitch and

roll angles of the fuselage. The body of revolution is discretized into fifteen sections longitudinally. Within each longitudinal section, four line sources/sinks are used to satisfy the zero normal velocity criterion at four control points located on the body of revolution as shown in Figure 4. The figure shows a cross section of a longitudinal section. The four line sources/sinks extend into the page and are denoted A, B, C and D. The four normal velocities at the control points are denoted V_1 through V_4. By changing the strengths of the sources/sinks, V_1 through V_4 are set identically to zero.

The combination of the two and three-dimensional sources/sinks influences the air velocity at the rotor blade producing an upwash on the forward part of the rotor and a downwash on the aft region. Additionally, the rotor wake geometry is distorted due to the presence of the fuselage. In this study, only the distortion of the concentrated tip vortices is considered and the inboard vortex sheet is not distorted due to the fuselage. This fuselage induced distortion required two major changes to the wake model: a wake displacement procedure and a modification to the wake distortion integration.

For both the prescribed wake and free wake cases, vortex lines that penetrate the fuselage surface are moved to place them outside of the fuselage. Similar to the procedure used in Ref. 22, if the endpoint of a vortex line segment is within the fuselage body, that endpoint is displaced vertically upward until it is at 110% of the fuselage radius. The additional 10% is what was chosen as the nominal value in Ref. 22. Whereas the vortex lines that penetrated the fuselage in Ref. 22 were subdivided into 10 smaller vortex lines, the vortex lines in the current study were not subdivided. To perform this procedure of resolution improvement would have required an entire redevelopment of the free wake code since the free wake code adapted from CAMRAD/JA [16] is not adaptable in this manner.

To model the influence of the rotor and wake on the fuselage aerodynamics, the pressure is integrated over the surface of the body of revolution and these forces are added to the drag forces calculated using the equivalent flat plate area. Since inviscid, incompressible flow is assumed and all streamlines originate in the steady, uniform free stream, fuselage pressures are related to velocities through Bernoulli's equation:

$$\frac{\partial \phi_V}{\partial t} + \frac{|V|^2}{2} + \frac{p}{\rho} = constant \tag{3}$$

The unsteady term, $\frac{\partial \phi_V}{\partial t}$, is neglected in this study and instead a correction to the total pressure is added to account for the energy added to the fluid by the rotor. As described in Ref. 2, a steady increment of $\Delta c_p = 2C_T/\mu^2$ is added to the pressure at fuselage locations within the rotor wake. The body of revolution is discretized into 60 panels. The pressure is determined at the center of each of these panels and is assumed constant over the area of the panel to determine the force acting on the panel. These contributions are added up so as to provide aerodynamic forces on the fuselage due to the rotor/wake.

3 METHOD OF SOLUTION

The calculation of the wake induced velocity influence coefficients is done in a wake loop outside of the coupled trim/aeroelastic response solution. This wake loop consists of three distinct wake approximations: (1) uniform inflow; (2) prescribed wake; and (3) free wake. Within each wake iteration, the coupled rotor/fuselage trim and aeroelastic response solutions are determined. The aeroelastic response of this system is obtained using the harmonic balance technique. In this study, the trim and response solutions are obtained simultaneously by satisfying the trim equilibrium and the vibratory response of the helicopter for all the rotor and fuselage degrees of freedom together. The equations of motion for the coupled rotor/fuselage system are concisely represented by:

$$\mathbf{F}_b(\mathbf{q}, \dot{\mathbf{q}}, \ddot{\mathbf{q}}, \mathbf{q}_t; \psi) = \mathbf{0} \tag{4}$$

$$\mathbf{F}_r(\mathbf{q}, \dot{\mathbf{q}}, \ddot{\mathbf{q}}, \mathbf{q}_t; \psi) = \mathbf{0} \tag{5}$$

$$\mathbf{F}_e(\mathbf{q}, \dot{\mathbf{q}}, \ddot{\mathbf{q}}, \mathbf{q}_t; \psi) = \mathbf{0} \tag{6}$$

$$\mathbf{F}_t(\mathbf{q}, \dot{\mathbf{q}}, \ddot{\mathbf{q}}, \mathbf{q}_t; \psi) = \mathbf{0} \tag{7}$$

Equation (4) represents the blade flap-lag-torsional equations of motion. The vectors $\mathbf{F}_r$, $\mathbf{F}_e$, and $\mathbf{F}_t$ correspond to the fuselage rigid body, the fuselage elastic motion expressed in modal domain, and the trim equations, respectively. The vector $\mathbf{q}_t$ represents the propulsive trim solution which consists of the quantities $\theta_o, \theta_{1c}, \theta_{1s}, \theta_{tr}$, α_R and ϕ_s. The response vector $\mathbf{q}$ consists of the blade, fuselage rigid body, and elastic degrees of freedom. The spatial dependence in the blade equations of motion is eliminated using Galerkin's method

based upon two torsional, two lag and three flap uncoupled, rotating free vibration modes. These rotating modes are obtained from a combination of the first nine exact nonrotating modes of a uniform cantilevered beam.

In steady and level forward flight, a periodic solution in the form of Fourier series is assumed for the blade and fuselage degrees of freedom [23,24]. The equations of motion are expanded in a Fourier series as:

$$\mathbf{F}_b = \mathbf{F}_{b_o} + \sum_{n=1}^{N_H} \{\mathbf{F}_{b_{nc}} cos(n\psi) + \mathbf{F}_{b_{ns}} sin(n\psi)\} \tag{8}$$

where

$$\begin{aligned} \mathbf{F}_{b_o} &= \frac{1}{2\pi} \int_0^{2\pi} \mathbf{F}_b(\mathbf{q}, \dot{\mathbf{q}}, \ddot{\mathbf{q}}, \mathbf{q}_t; \psi)\, d\psi \\ \mathbf{F}_{b_{nc}} &= \frac{1}{\pi} \int_0^{2\pi} \mathbf{F}_b(\mathbf{q}, \dot{\mathbf{q}}, \ddot{\mathbf{q}}, \mathbf{q}_t; \psi) cos(n\psi)\, d\psi \\ \mathbf{F}_{b_{ns}} &= \frac{1}{\pi} \int_0^{2\pi} \mathbf{F}_b(\mathbf{q}, \dot{\mathbf{q}}, \ddot{\mathbf{q}}, \mathbf{q}_t; \psi) sin(n\psi)\, d\psi \end{aligned} \tag{9}$$

Similar equations apply to the fuselage rigid and elastic equations of motion. (The trim equations are the same as the constant part of the fuselage equations). These integrals over the azimuth describing the Fourier coefficients are determined using Gaussian quadrature. The set of trim, blade, fuselage rigid body, and elastic equations are combined and solved simultaneously for steady and level forward flight to yield the required solution vector. This system of equations is solved by the IMSL nonlinear algebraic equation solver, DNEQNF [20]. This routine uses the Levenberg-Marquardt algorithm to solve the trim/aerodynamic response simultaneously and calculates the Jacobian of the system using a finite difference scheme.

As described in the mathematical formulation of the wake model, the wake calculation routine returns influence matrices that relate the inflow distribution to the circulation distribution. However the circulation distribution is dependent on the required lift and the lift is dependent on the inflow distribution. Thus it is necessary to iterate on circulation convergence. Given the circulation distribution from the previous iteration, the inflow distribution is determined. From the inflow distribution, the distribution of lift is calculated. From the calculated lift, the required circulation is determined and the process repeats until the circulation converges within a prescribed limit.

4 CONTROL APPROACH

The coupled rotor/flexible fuselage model contains a provision for an ACSR system by mounting the rotor on a rigid plate. This rigid plate is connected to the fuselage with high force/small displacement actuators as shown in Figure 2. The corners of this plate are denoted P2, P4, P6 and P8. The actuators are connected to the fuselage at points P1, P3, P5 and P7. Control inputs are fed to these actuators at the rotor disturbance frequency (N_b/rev) in order to counteract the rotor forcing and minimize vibrations at selected fuselage locations such as the pilot seat and rear cabin.

The basic control strategy used in this study is described in detail in Ref. 14. Springs, used as a control parameter to distribute weighting between control power and control effectiveness, are introduced parallel to the actuators at the four corners of the rigid plate. The forces across the servo actuators, due to control inputs and spring forces caused by fuselage elastic deformation, are set to zero through the proper choice of control inputs. This in turn reduces overall airframe vibrations.

An improved control strategy based on the minimization of a performance index has been implemented. This is an adaptation of a control strategy used in previous HHC and IBC studies [8,25]. The performance index used in this study is a quadratic function of selected acceleration amplitudes $\vec{z}$ and control amplitudes $\vec{u}$.

$$J = \vec{z}^T \mathbf{W}_z \vec{z} + \vec{u}^T \mathbf{W}_u \vec{u} \tag{10}$$

The weighting matrices, $\mathbf{W_z}$ and $\mathbf{W_u}$, allow relative importance to be assigned to the components of acceleration at various locations and the control inputs. It is therefore possible to choose which degrees of freedom are most important and tailor the vibration reduction method to preferentially reduce those accelerations.

The optimal control is found by setting the gradient of the performance index J with respect to the control $\vec{u}$ to zero:

$$\frac{\partial J}{\partial \vec{u}} = 0 \tag{11}$$

To determine the gradient of the performance index with respect to the control, it is necessary to know the gradient of the accelerations with respect to the control. To this end, the accelerations are linearized about the current control input $\vec{u}_i$

$$\vec{z}(\vec{u}) = \vec{z}(\vec{u}_i) + \mathbf{T}_i(\vec{u} - \vec{u}_i) \tag{12}$$

where

$$\mathbf{T} = \frac{\partial \vec{z}}{\partial \vec{u}} \tag{13}$$

The transfer matrix $\mathbf{T}$ is the Jacobian of the acceleration response with respect to the current control input. This Jacobian is calculated numerically using the finite difference method.

Substituting this model of the acceleration response in the the performance index and minimizing with respect to the control produces

$$\vec{u}^*_{i+1} = -\mathbf{D}_i^{-1}\mathbf{T}_i^T\mathbf{W}_\mathbf{z}[\vec{z}_i - \mathbf{T}_i\vec{u}^*_i] \tag{14}$$

where

$$\mathbf{D}_i = \mathbf{T}_i^T\mathbf{W}_\mathbf{z}\mathbf{T}_i + \mathbf{W}_\mathbf{u} \tag{15}$$

This system is similar to the local controller described in References 25 and 15. This procedure can be started by setting the initial optimal control input to zero and repetitively applying Eq. 14 until the optimal control input converges. The resulting control vector is the optimal control vector for the given weighting matrices.

5 RESULTS AND DISCUSSION

In this study, a coupled rotor/flexible fuselage model resembling the MBB BO-105 helicopter is chosen. The non-dimensional properties are provided in in Table 1. The fuselage natural modes are coupled modes so the descriptions given in the table are qualitative and are not meant to denote classical yawing, pitching and torsional modes.

Figures 5 - 7 compare the vibratory hub shears obtained from the various aerodynamic models. Five distinct aerodynamic models are considered. The first two aerodynamic models are uniform inflow and the free wake model. The description 'fuselage aero 1' refers to the first refinement of the fuselage aerodynamic model. In this stage, sources/sinks are included to influence the velocities at the rotor blades which in turn influence the rotor loads. However, this version of the aerodynamic model lacks the integration of the pressures over the fuselage surface to account for rotor aerodynamic influences on the fuselage. 'Fuselage aero 2' is the second refinement of the model and includes the aforementioned sources/sinks as well as the integration of pressure over the fuselage surface. 'Fuselage aero 3' is the third refinement of the model. It includes the distortion of the wake due to the fuselage in addition to all previously described effects. This produces fully coupled rotor/fuselage aerodynamic interactions. As seen in the figures, vibratory hub shears obtained with the free wake model are significantly higher than the uniform inflow results, especially at lower advance ratios where blade vortex interaction plays a larger role. The inclusion of fuselage interference effects on the rotor results in vibratory loads significantly higher than that obtained with the free wake model alone. The second and third refinements of the fuselage aerodynamic model have little to no affect on the hub shears in the longitudinal and lateral directions. In the vertical direction, the inclusion of wake distortion affects due to the fuselage significantly alters the vibratory hub loads. Above an advance ratio of $\mu = 0.25$, the vertical vibratory hub shear when using the third refinement of the fuselage aerodynamic model is up to 100% larger than the free wake model alone. The vibratory hub moments show similar trends as the lateral and longitudinal shears.

Figures 8 and 9 show the 4/rev accelerations at the pilot seat and at a rear cabin position as a function of advance ratio. In both figures, the accelerations are shown for two different aerodynamic models: the uniform inflow model and the free wake model. The accelerations obtained using the free wake model are much higher than the uniform inflow results. As in the studies by Yeo and Chopra, at low advance ratios the accelerations at the pilot seat are shown to be orders of magnitude greater when using the free wake model. In Ref. 1, the effect of the free wake model is shown to result in an approximately constant increase to the vibration levels at advance ratios of 0.2 and above. However in our study, this increase diminishes at these higher advance ratios.

The location where accelerations are measured plays a significant role in the magnitude of the accelerations as evident from comparing the two figures.

Figures 10 and 11 compare the acceleration levels obtained using uniform inflow to those obtained using the free wake model with the addition of rotor/fuselage interaction effects. In Fig. 10, the pilot seat accelerations are plotted and the rear cabin accelerations are shown in Fig. 11. Large increases are noted in all accelerations with the inclusion of refined aerodynamics but are most notable in the pilot seat vertical and lateral accelerations and the rear cabin vertical accelerations. The effect is apparent at all advance ratios. The accelerations obtained using the free wake model alone are similar to those obtained with the inclusion of rotor/fuselage aerodynamic interactions at low advance ratios. At higher advance ratios, the inclusion of rotor/fuselage aerodynamic interactions results in accelerations that are up to 100% greater than those of the free wake model alone. At higher advance ratios, the influence of the wake on the rotor aerodynamic loads diminishes while the relative influence of the fuselage on the rotor increases.

The ability of the weighted control algorithm to drastically reduce airframe vibrations are shown in Figs. 12 to 14. These results were obtained without penalizing either the actuator force or actuator power requirements. This provides a best case scenario for vibration reduction if there are no practical constraints on the actuator system. The longitudinal accelerations for the controller both engaged and disengaged are shown in Fig. 12. For both airframe locations, vibrations are reduced by 45% to 68%. In the lateral direction, Fig. 13 shows vibrations at both locations to be almost completely eliminated when the controller is active. Pilot seat accelerations are reduced to between 1.0% and 1.6% of the uncontrolled values. Similarly, rear cabin lateral accelerations are reduced to between 1.8% and 3.3% of the uncontrolled values. The vertical accelerations are shown in Fig. 14. Again the accelerations are nearly eliminated by the controller. Pilot seat accelerations with the controller active are 2.8%-4.1% of the uncontrolled values. Rear cabin accelerations are 0.2%-0.3% of the uncontrolled values. Using the weighted control algorithm, accelerations at selected locations can be reduced to levels that are two orders of magnitude less than the uncontrolled values. But this near complete vibration elimination is accompanied by prohibitive power and actuator force requirements. With no control penalty, the actuators require between 2% and 15% of total rotor power and need to exert up to 40000 lbs force.

The weighted control method with practical constraints on the actuator forces and power, to model a feasible control scheme, is compared to the basic control scheme in Figs. 15 to 18. The longitudinal acceleration levels for both the pilot seat and the rear cabin location are shown for each control method in Fig. 15. The accelerations of the two airframe locations are nearly the same in this direction. Though the basic controller provides better vibration reduction at $\mu = 0.15$, the vibration levels are low for both control methods at this point. For higher advance ratios, $\mu \geq 0.20$, the weighted control method reduces vibrations further than the basic controller. The accelerations obtained using the weighted control method are up to 74% less than the basic control method accelerations.

In the lateral direction, shown in Fig. 16, the basic control scheme is ineffective in reducing accelerations. The accelerations obtained using the weighted controller are lower than the basic control accelerations at all advance ratios. The weighted control method provides rear cabin accelerations that are 19% to 50% lower than the basic control accelerations. Pilot seat lateral accelerations with the weighted control method are a minimum of 56% below the basic control accelerations and are reduced up to 81% at certain advance ratios. This reduction is especially noticeable at high advance ratios where the weighted control accelerations are 26% of the basic control accelerations at an advance ratio of $\mu = 0.40$.

The vertical pilot seat and rear cabin acceleration levels are shown in Fig. 17. The weighted control accelerations are lower than the basic control accelerations at all advance ratios for both airframe locations. The weighted control vertical acceleration levels at the pilot seat are from 34% lower than the basic control acceleration levels at low advance ratios, $\mu = 0.15$, to 49% lower at high advance ratios, $\mu = 0.40$. The greatest reduction is at $\mu = 0.30$ where the weighted control accelerations are 66% less than the basic control accelerations. At the rear cabin position, the weighted control method reduces accelerations to levels that are a minimum of 69% below and up to 82% below the basic control accelerations. At $\mu = 0.40$, the basic control method is only able to reduce vibrations at the rear cabin to 0.16g where the weighted control method reduces vibrations to 0.035g. This is a significant additional reduction that helps to meet the goal of a "jet smooth ride".

The power requirements of the two control schemes are compared in Fig. 18. The actuator power requirements are shown as a percentage of main rotor power. The two control methods have similar power requirements. Whereas the basic control method needs a greater percentage of rotor power as advance ratio increases, the weighted control method requires a relatively constant percentage of 1.5% of rotor power. Both

control schemes require actuators able to produce forces on the order of 6000 lbs at high advance ratios.

6 CONCLUDING REMARKS

A free wake model and a fuselage aerodynamic model capable of simulating rotor/fuselage aerodynamic interactions has been combined with a coupled rotor/flexible fuselage model to study vibrations and their reduction using ACSR. A control approach has been developed that preferentially reduces accelerations at prescribed airframe locations. This control method has been compared to an earlier control approach studied at UCLA. The results represent an important contribution towards vibration predictions and cost effective vibration reduction using the ACSR approach. Several conclusions are summarized below:
(1) Refined aerodynamics significantly affect the vibratory loads transfered from the rotor to the fuselage and the accelerations experienced at various fuselage locations.
(2) A free wake model and the inclusion of fuselage aerodynamic effects on the rotor and wake are necessary for vibration prediction at all forward speeds. The inclusion of rotor aerodynamic effects on the fuselage plays a minor roll in the production of vibrations.
(3) Accelerations obtained using the free wake model and including rotor/fuselage aerodynamic interactions are orders of magnitude greater than those obtained using uniform inflow at lower advance ratios and are significantly greater at higher advance ratios.
(4) The weighted control algorithm with no control penalty was able to nearly eliminate all acceleration components at the pilot seat and rear cabin position for all advance ratios. This exceptional vibration reduction capability required a prohibitive amount of control power and actuator force amplitude.
(5) Both the basic controller and the weighted controller with control penalty were unable to reduce lateral accelerations at the rear cabin position. A better alignment of actuators could allow for the reduction of these accelerations with realistic actuator requirements.
(6) The weighted control algorithm with control penalty was able to reduce accelerations at the desired locations significantly below the accelerations of the basic control scheme using similar actuator forces and power. The accelerations obtained using the weighted controller were up to 82% below the basic controller accelerations.

ACKNOWLEDGMENTS

This research is supported by the U.S. Army Research Office under grant No. DAAH04-95-1-0320 with Dr. Gary Anderson as grant monitor.

References

[1] Yeo, H. and Chopra, I. , "Modeling Issues Related to Vibration Prediction of a Coupled Rotor/Fuselage System," AIAA Paper No. 97-1212, Proceedings of the 38th AIAA/ASME/ASCE/AHS/ASC Structures, Structural Dynamics and Materials Conference, Kissimmee, FL, April 1997, pp. 2739–2751.

[2] Lorber, P. F. and Egolf, T. A. , "An Unsteady Helicopter Rotor/Fuselage Interaction Analysis," NASA CR-4178, September 1988.

[3] Mavris, D. N. , Komerath, N. M. , and McMahon, H. M. , "Prediction of Aerodynamic Rotor-Airframe Interactions in Forward Flight," *Journal of the American Helicopter Society*, October 1989, pp. 37–46.

[4] Berry, J. and Bettshart, N. , "Rotor-Fuselage Interaction: Analysis and Validation with Experiment," Proceedings of the 53rd Annual Forum of the American Helicopter Society, Virginia Beach, VA, 1997, pp. 343–367.

[5] Smith, C. A. and Betzina, M. D. , "Aerodynamic Loads Induced by a Rotor on a Body of Revolution," *Journal of the American Helicopter Society*, January 1986, pp. 29–36.

[6] Leishman, J. G. and Bi, N. , "Aerodynamic Interactions Between a Rotor and a Fuselage in Forward Flight," *Journal of the American Helicopter Society*, July 1990, pp. 22–31.

[7] Bi, N. and Leishman, J. G. , "Experimental Study of Rotor/Body Aerodynamic Interactions," *Journal of Aircraft*, Vol. 27, No. 9, September 1990, pp. 779–788.

[8] Friedmann, P. P. and Millott, T. A. , "Vibration Reduction in Rotorcraft Using Active Control: A Comparison of Various Approaches," *Journal of Guidance, Control, and Dynamics*, Vol. 18, No. 4, 1995, pp. 664–673.

[9] King, S. P. and Staple, A. E. , "Minimization of Helicopter Vibration Through Active Control of Structural Response," Rotorcraft Design Operations, AGARD-CP-423, October 1986, pp. I4–1 – I4–13.

[10] Staple, A. E. , "An Evaluation of Active Control of Structural Response as a Means of Reducing Helicopter Vibration," Proceedings of the 15th European Rotorcraft Forum, Amsterdam, Netherlands, September 1989, pp. 3–17.

[11] Welsh, W. A. , von Hardenberg, P. C. , von Hardenberg, P. W. , and Staple, A. E. , "Test and Evaluation of Fuselage Vibration Utilizing Active Control of Structural Response (ACSR) Optimized to ADS-27," Proceedings of the 46th Annual Forum of the American Helicopter Society, Washington, DC, may 1990, pp. 21–37.

[12] Welsh, W. A. *et al.*, "Flight Test on an Active Vibration Control System on the UH60 Black Hawk Helicopter," Proceedings of the 51st Annual Forum of the American Helicopter Society, Fort Worth, TX, may 1995, pp. 393–402.

[13] Chiu, T. and Friedmann, P. P. , "A Coupled Helicopter Rotor-Fuselage Aeroelastic Response Model for ACSR," AIAA Paper No. 95-1226, Proceedings of the 36th AIAA/ASME/ASCE/AHS/ASC Structures, Structural Dynamics and Materials Conference, New Orleans, LA, April 1995, pp. 574–600.

[14] Chiu, T. and Friedmann, P. P. , "ACSR System for Vibration Suppression in Coupled Rotor-Flexible Fuselage Model," AIAA Paper No. 96-1547, Proceedings of the 37th AIAA/ASME/ASCE/AHS/ASC Structures, Structural Dynamics and Materials Conference, Salt Lake City, UT, April 1996, pp. 1972–1991.

[15] Millott, T. A. and Friedmann, P. P. , "Vibration Reduction in Helicopter Rotors Using an Actively Controlled Partial Span Trailing Edge Flap Located on the Blade," NASA CR-4611, 1994.

[16] Johnson, W. , A Comprehensive Analytical Model of Rotorcraft Aerodynamics and Dynamics, Vol. I: Theory Manual. Johnson Aeronautics, Palo Alto, CA, 1988.

[17] Johnson, W. , A Comprehensive Analytical Model of Rotorcraft Aerodynamics and Dynamics, Vol. II: User's Manual. Johnson Aeronautics, Palo Alto, CA, 1988.

[18] Scully, M. P. , "Computation of Helicopter Rotor Wake Geometry and its Influence on Rotor Harmonic Airloads," Ph.D. Dissertation, Aeroelastic Research Laboratory, Massachusetts Institute of Technology, 1975.

[19] Johnson, W. , "Wake Model for Helicopter Rotors in High Speed Flight," NASA CR-177507, 1988.

[20] _, IMSL Library: Reference Manual. IMSL Inc., Houston, TX, 1980.

[21] Rand, O. and Gessow, A. , "Model for Investigation of Helicopter Fuselage Influence on Rotor Flowfields," *Journal of Aircraft*, Vol. 26, No. 5, May 1989, pp. 401–402.

[22] Lorber, P. F. and Egolf, T. A. , "An Unsteady Helicopter Rotor-Fuselage Aerodynamic Interaction Analysis," *Journal of the American Helicopter Society*, July 1990, pp. 32–42.

[23] Millott, T. A. and Friedmann, P. P. , "Vibration Reduction in Helicopter Rotors Using an Active Control Surface Located on the Blade," AIAA Paper No. 92-2451, Proceedings of the 33rd AIAA/ASME/ASCE/AHS/ASC Structures, Structural Dynamics, and Materials Conference, Dallas, TX, April 1992, pp. 1975–1988.

[24] Papavassiliou, I. , Friedmann, P. P. , and Venkatesan, C. , "Coupled Rotor/Fuselage Vibration Reduction Using Open-Loop Blade Pitch Control," *Mathematical Computer Modeling*, Vol. 18, No. 3, 1993, pp. 131–156.

[25] Johnson, W. , "Self-Tuning Regulators for Multicyclic Control of Helicopter Vibrations," NASA TP-1996, 1982.

Rotor Data	
$EI_y/m_b\Omega^2R^4 = 0.0106$	
$EI_z/m_b\Omega^2R^4 = 0.0301$	
$GJ/m_b\Omega^2R^4 = 0.001473$	
$N_b = 4$	$a = 2\pi$
$\gamma = 5.5$	$\beta_p = 0.0$
$\sigma = 0.07$	$c_b/R = 0.055$
Helicopter Data	
$C_W = 0.0050$	$fC_{d_f}/\pi R^2 = 0.01$
$Z_{FC}/R = 0.2851$	$Z_{FA}/R = 0.2851$
$X_{FC}/R = 0.0$	$X_{FA}/R = 0.0$
$h/R = 0.0931$	$I_x/m_bR^2 = 4.2216$
$I_y/m_bR^2 = 10.7781$	$I_z/m_bR^2 = 7.9366$

Fuselage Mode Shape Description and Frequency(Hz)	
Fuselage yawing	5.28
Fuselage pitching	5.36
Fuselage torsion	11.07
Fuselage compression	18.81
Tail boom bending	23.23
Fuselage torsion	25.11
Landing gear vertical	26.73
Landing gear lateral	29.02

Table 1: Helicopter Data

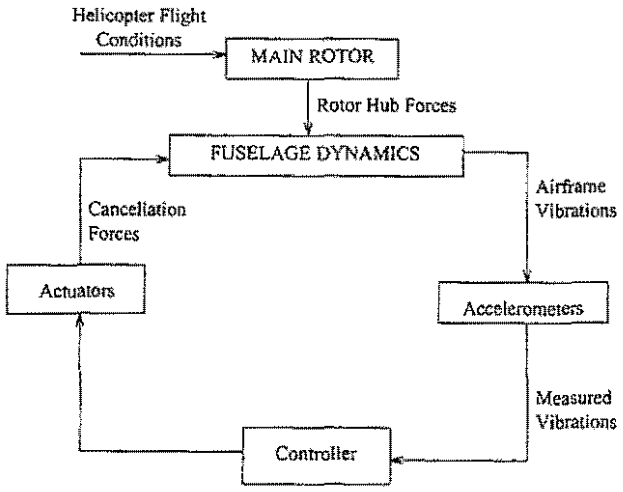

Figure 1: Helicopter System Schematic for ACSR

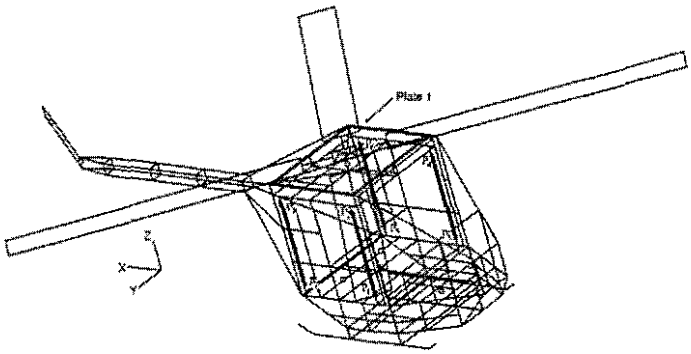

Figure 2: Coupled Rotor/Active Control/Fuselage Dynamic System

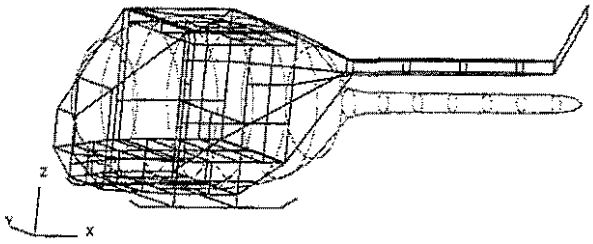

Figure 3: Body of Revolution/Fuselage Comparison

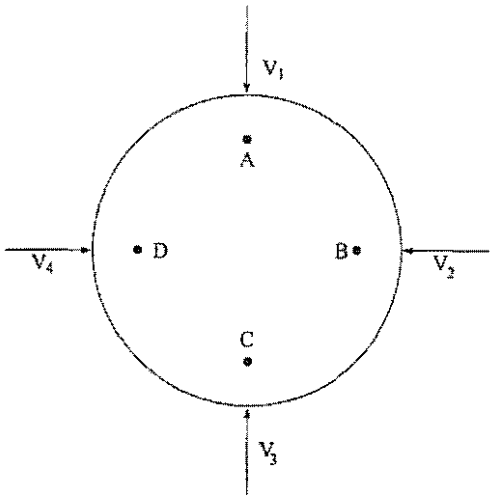

Figure 4: Cross Section of Body of Revolution

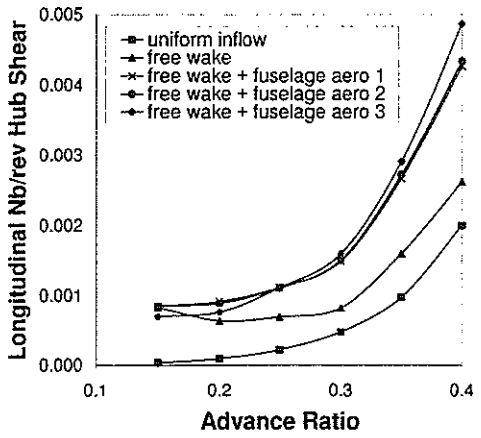

Figure 5: Longitudinal N_b/rev Hub Shears

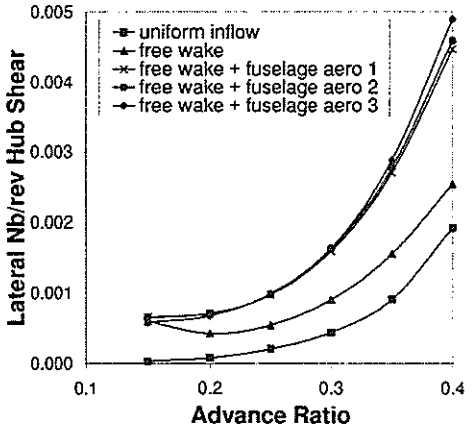

Figure 6: Lateral N_b/rev Hub Shears

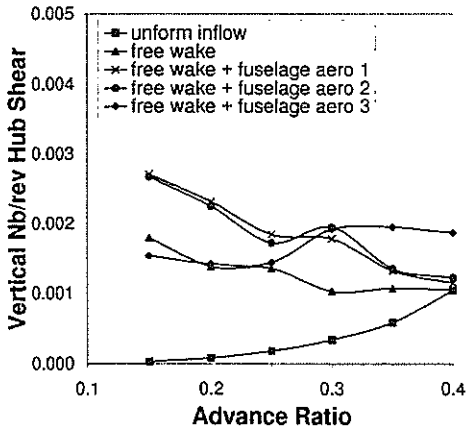

Figure 7: Vertical N_b/rev Hub Shears

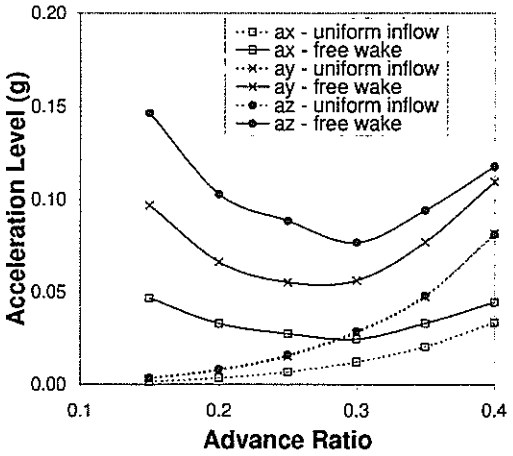

Figure 8: 4/Rev Accelerations at the Pilot Seat

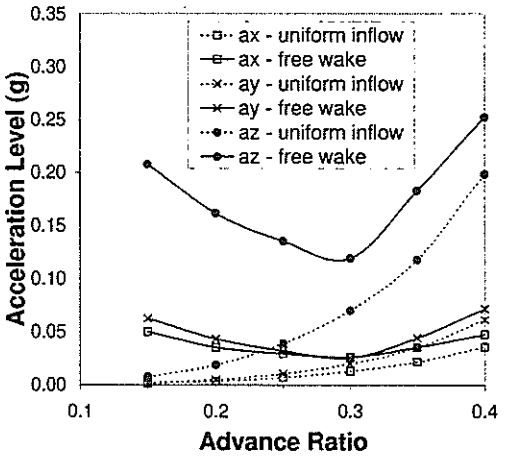

Figure 9: 4/Rev Accelerations at a Rear Cabin Position

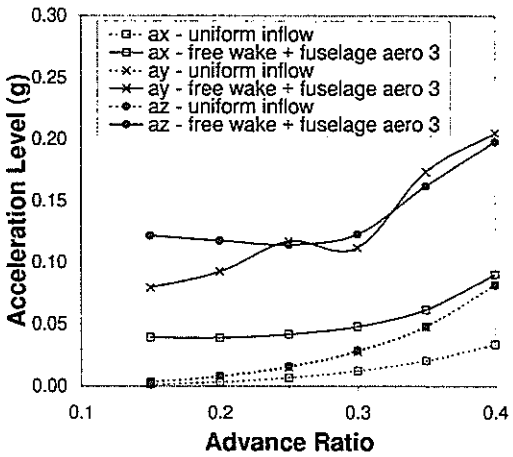

Figure 10: 4/Rev Accelerations at the Pilot Seat

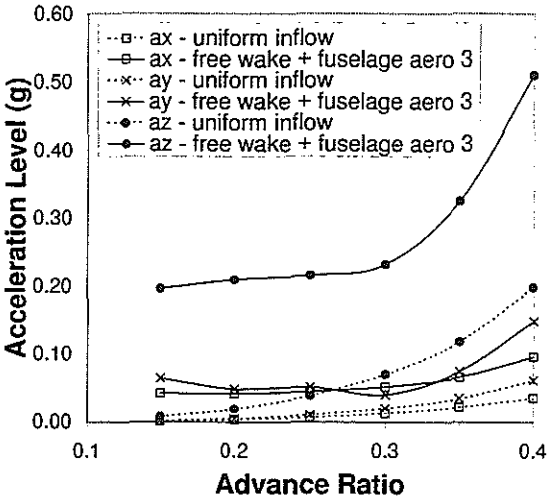

Figure 11: 4/Rev Accelerations at a Rear Cabin Position

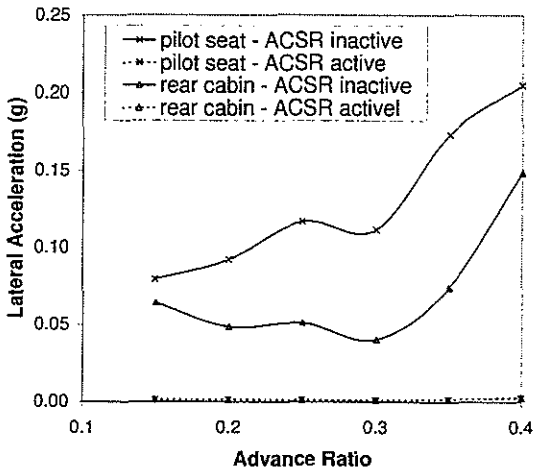

Figure 13: Lateral Accelerations, Weighted Controller with No Control Penalty

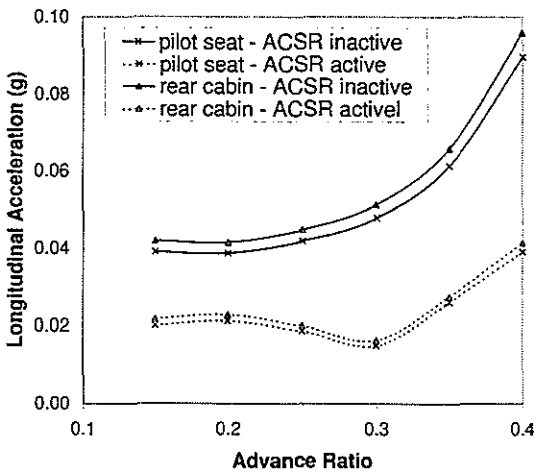

Figure 12: Longitudinal Accelerations, Weighted Controller with No Control Penalty

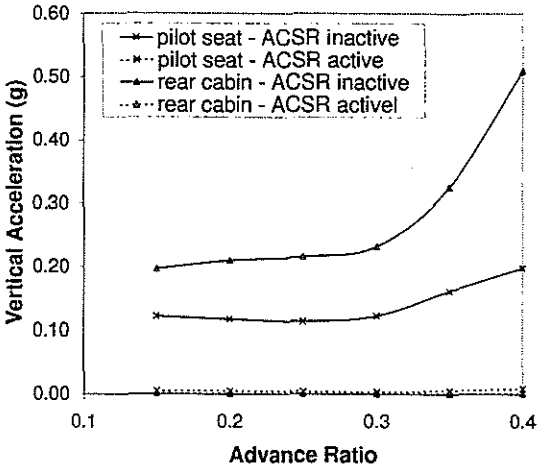

Figure 14: Vertical Accelerations, Weighted Controller with No Control Penalty

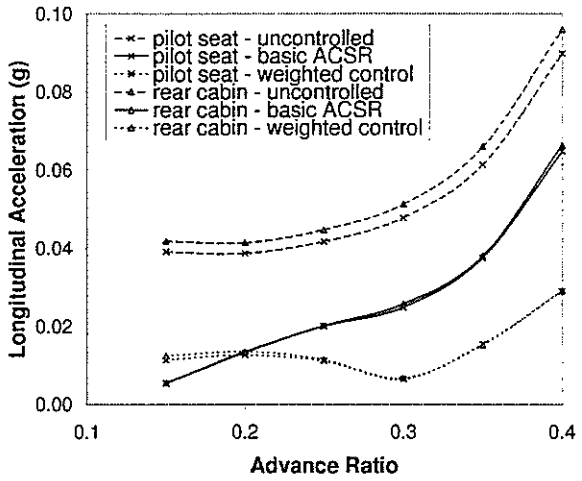

Figure 15: Longitudinal accelerations, comparison of control schemes

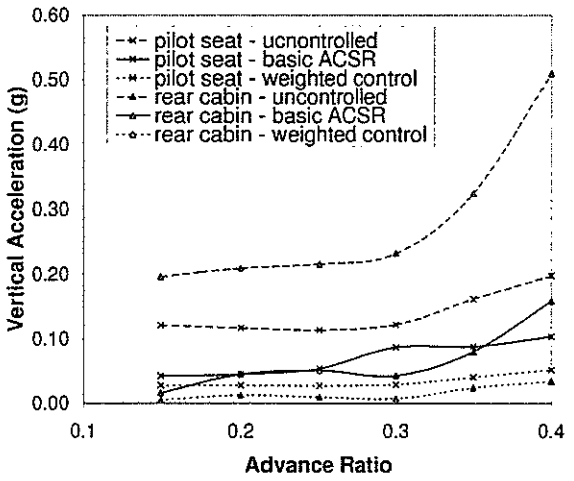

Figure 17: Vertical accelerations, comparison of control schemes

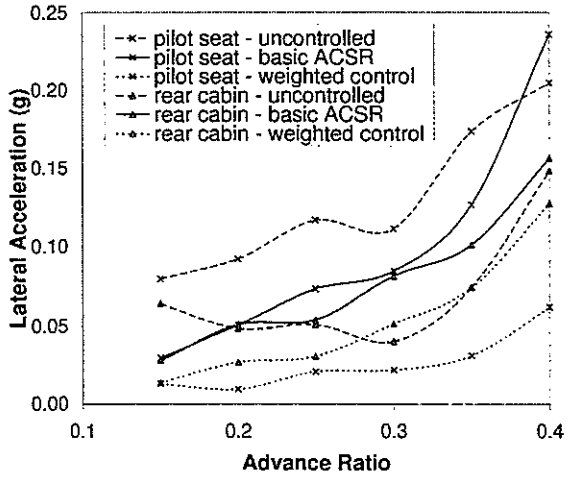

Figure 16: Lateral accelerations, comparison of control schemes

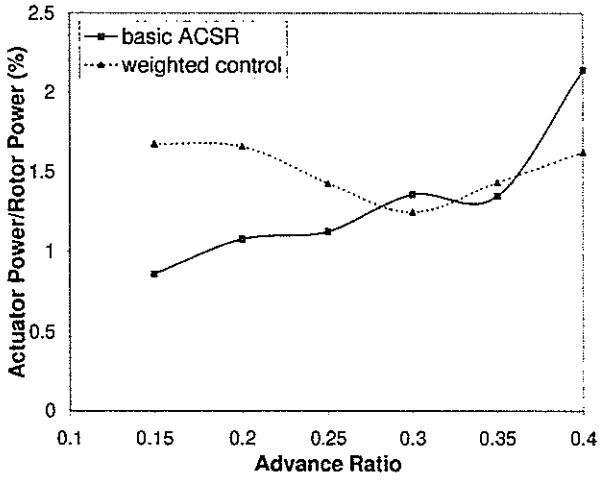

Figure 18: Power requirements, comparison of control schemes